JOURNAL OF CATALYSIS 85, 206–223 (1984)

Surface Structure and Temperature Dependence of *n*-Hexane Skeletal Rearrangement Reactions Catalyzed over Platinum Single Crystal Surfaces: Marked Structure Sensitivity of Aromatization

S. MARK DAVIS,[1] FRANCISCO ZAERA, AND GABOR A. SOMORJAI

Materials and Molecular Research Division, Lawrence Berkeley Laboratory, and Department of Chemistry, University of California, Berkeley, Berkeley, California, 94720

Received April 5, 1983; revised August 1, 1983

The surface structure and temperature dependence of *n*-hexane skeletal rearrangement was investigated near atmospheric pressure and at 520–700 K over a series of five platinum single crystal surfaces with variable terrace, step, and kink structures. The atomic structure and surface composition of the active catalyst was determined before and after reactions using low energy electron diffraction and Auger electron spectroscopy. Aromatization of *n*-hexane to benzene displayed unique structure sensitivity in which the rates and specificity for this important reforming reaction were maximized on platinum surfaces with hexagonal (111) terrace structure. The rates of competing isomerization, C_5-cyclization, and hydrogenolysis reactions displayed little dependence on surface structure, although hydrogenolysis product distributions were influenced markedly by terrace structure. Platinum surfaces with (100) terraces favored internal C–C bond scission, whereas surfaces with (111) terraces displayed high selectivity for terminal hydrogenolysis. Skeletal rearrangement was dominated by cyclic mechanisms involving both 1,5- and 1,6-ring closure. Marked variations in reaction selectivity with reaction conditions are related to a change of the most abundant surface intermediate that results from changes in the surface concentration of chemisorbed hydrogen. Catalyst deactivation resulted from the formation of disordered carbonaceous deposits on the platinum surfaces whose primary role was that of a nonselective poison.

1. INTRODUCTION

Skeletal rearrangement reactions of *n*-hexane have been investigated over many types of platinum catalysts including powders (*1–3*), films (*4*), Pt/SiO_2 (*5*), Pt/Al_2O_3 (*6–8*), supported alloys including PtCu (*9*), PtPd (*10, 11*), PtRe (*12*), PtSn (*13*), and PtAu (*14–16*), and also over other Group VIII metals such as Ni and NiCu powders (*17*), Ir and IrAu films (*18*), and supported Pd, PdAu, Rh, and RhCu catalysts (*16, 19*). Dautzenberg and Platteeuw (*7, 8*) and Ponec and co-workers (*5*) found no significant structure sensitivity for *n*-hexane reactions catalyzed at 1–10 atm and 530–760 K over Pt/SiO_2 and monofunctional Pt/Al_2O_3 catalysts. This conclusion resulted from studies of the isomerization and cyclization rates as a function of the average platinum particle size which was varied between about 15 and 80 Å. Anderson (*4*) and Santacessaria (*2*), by contrast, reported significant variations in catalytic activity for ultra thin films and Pt/SiO_2 catalysts where very small 10 Å crystallites appeared to be at least 3–5 times more active than larger platinum particles for *n*-hexane isomerization (*4*) and/or hydrogenolysis and C_5-cyclization (*2, 4*). These changes in catalytic behavior with platinum dispersion were interpreted in terms of the different "cyclic" ((*20–26*) and references in (*21*)) and "bond-shift" (*26–28*) mechanisms that prevail on the very small and larger platinum particles, respectively.

To obtain more detailed information about the structure sensitivities of alkane skeletal rearrangement reactions, model

[1] Permanent address: Exxon Research and Development Laboratory, P.O. Box 2226, Baton Rouge, La. 70821.

0021-9517/84 $3.00

catalytic studies have been carried out in this laboratory using small area platinum single crystal surfaces that possess well-defined atomic structure and surface composition (*29–34*). Studies by Gillespie (*29*) *et al.* of *n*-heptane aromatization and hydrogenolysis catalyzed near atmospheric pressure for example, revealed that the rates and selectivities of these reactions are influenced strongly by the presence of surface irregularities (atomic steps and kinks) on the platinum surfaces. Aromatization activities and selectivities were maximized on stepped and kinked surfaces with hexagonal terraces of (111) orientation that were wide enough (4–5 atoms) to accept chemisorbed reactants, intermediates and products. Hydrogenolysis exhibited a different dependence upon surface structure in which the flat (111) and highly stepped-kinked (*25, 10, 7*) surfaces were most active for this undesirable C–C bond breaking reaction. For other reactions such as the bond-shift isomerization of butanes and neopentane (*31*), high concentrations of square (100) microfacets were essential for high catalytic activity.

Here we report studies of *n*-hexane skeletal rearrangement reactions catalyzed near atmospheric pressure and at 500–700 K over a series of five platinum single crystal surfaces with variable terrace, step, and kink structures. The studies have confirmed that aromatization rates are very sensitive to surface structure; crystal faces with hexagonal terrace structure lead to maximum aromatization specificity. By contrast, the rates of the competing hydrogenolysis, isomerization, and C_5-cyclization reactions displayed little dependence on the atomic arrangement of the platinum surface. Temperature and hydrogen pressure exerted a more decisive influence in controlling the rates and selectivities of *n*-hexane skeletal rearrangement. For certain reactions such as aromatization and bond-shift isomerization, it now appears certain that high selectivity can be predictably tailored with appropriate choice of the reaction conditions and the platinum atomic surface structure.

2. EXPERIMENTAL

All of the experiments were carried out in an ultrahigh vacuum–high pressure apparatus described previously (*29–31*) that is designed for combined surface analysis and catalysis studies using small area samples. This system was equipped with four-grid electron optics for low energy electron diffraction (LEED) and Auger electron spectroscopy (AES), an argon ion gun for crystal cleaning, a quadrupole mass spectrometer, and a retractable internal isolation cell which operates as a well-mixed microbatch reactor in the 10^{-2}–10 atm pressure range. The reaction cell and external recirculation loop were connected to an isolable Wallace & Tiernan gauge, a bellows pump for gas circulation, and a gas chromatograph sampling valve. Hydrocarbon conversion was monitored with an HP 3880 gas chromatograph calibrated with CH_4/N_2 mixtures.

Idealized atomic surface structures for the single crystal samples used in this research are shown in Fig. 1. Miller indices, average terrace widths, kink concentrations, and microfacet indices for these surfaces are summarized in Table 1. In the microfacet notation (*35*) the terms $a_b(hkl)$ describe the number b and type (hkl) of terrace, step, and kink microfacets contained in the unit cell of the surface. All the single crystal samples were prepared as thin (<0.5 mm) disks so that the polycrystalline edges would contribute no more than 10–16% of the total platinum surface area (≈1 cm^2). The total area was used in the calculation of all reaction rates. Research purity *n*-hexane (Phillips >99.99 mol%) and hydrogen (LBL-Matheson, >99.998%) were used as supplied after outgassing the former by repeated freeze pumping cycles at ~77 K.

The single crystals were spotwelded to a rotatable manipulator using a series of platinum, gold and copper supports (*30*) that enabled the samples to be resistively heated to

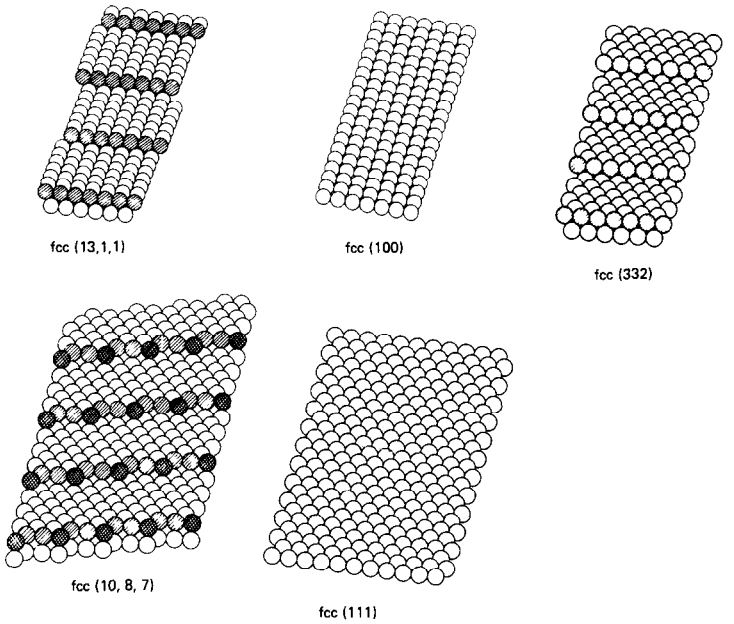

FIG. 1. Idealized atomic structures for platinum single crystal surfaces.

about 1400 K without significant heating of any other part of the reaction chamber. The samples were repeatedly mounted and remounted until heating was uniform and the sample contact points were no hotter than the crystal itself (the contacts represent only 1–2% of the total Pt area). Both crystal faces were cleaned using repeated cycles of argon ion-sputtering, oxygen pretreatment and annealing at 1050–1350 K, until the surface structure was well defined by LEED, and surface impurities such as Ca, Si, P, S, O, and C were no longer detectable by AES. Subsequently, the reaction cell was closed in seconds and pressurized to about 1 atm with H_2 to cool the sample and supports below 330 K. After about 1 min, the hydrogen was removed, hydrocarbon vapor and hydrogen were reintroduced to desired pressures, circulation was commenced, and the crystal was heated to the reaction temperature over a period of about 1 min. The reaction temperature was continuously regulated to ±2 K using a preci-

TABLE 1

Miller Indices, Average Terrace Widths, and Microfacet Indices for Platinum Single Crystal Surfaces

Miller index	Terrace width (Å)	Microfacet index[a]
Pt(100)	—	Pt(100)
Pt(111)	—	Pt(111)
Pt(332)	14.0	Pt(S) − [5/2 $_5$(111) + 1 $_1$(11$\bar{1}$)]
Pt(13,1,1)	18.0	Pt(S) − [12 $_6$(100) + 1 $_1$(111)]
Pt(10,8,7)[b]	15.1	Pt(S) − [15/2 $_{15}$(111) + 2 $_2$(100) + 1 $_1$(11$\bar{1}$)]

[a] For a detailed explanation see Ref. (7).

[b] Kink concentration = 1×10^{14} atoms cm^{-2} (i.e., ~6% kinks).

sion temperature controller referenced to a chromel–alumel thermocouple spotwelded to an edge or face of the crystal. As discussed elsewhere (*31*), high levels of both accuracy and precision in the temperature measurements from one crystal to another were insured from measurements of the equilibrium isobutene yields produced in isobutane reaction studies using the same platinum crystals.

At the end of the reaction rate studies, the samples were cooled to below 320 K, the reaction mixture was removed, the reaction cell was opened, and Auger spectra were immediately recorded, all within a period of about 10 min. Contamination of the surface by impurities such as sulfur and chlorine was not observed.

Initial reaction rates were determined graphically from the slopes of product accumulation curves determined as a function of reaction time. Initial rates and selectivities in repeat experiments were reproducible to about ±20 and ±5%, respectively. Reproducibility of reaction rates and selectivities with different crystals of the same orientation were better than ±30 and ±10%, respectively. Blank reaction studies, carried out over surfaces covered with graphitic carbon deposits that formed upon heating in hydrocarbon at 750–800 K, revealed a very low level of background catalytic activity corresponding to 2–4% of the activity measured for initially clean platinum.

It should be noted that the clean (100) and (13,1,1) platinum crystal faces display surface reconstructions that can be approximately represented by (5 × 20) coincidence lattice structures (*36, 37*). Dynamical LEED intensity calculations (*37*) for Pt(100) suggest that the topmost surface layer is hexagonal, buckled, and contracted about 6% with respect to the bulk metal *d*-spacing. Upon exposure to hydrocarbons at high or low pressures we have always observed (1 × 1) structures indicative of the unreconstructed (100) and (13,1,1) crystal faces. Since hydrocarbon catalysis appears to occur on these unreconstructed surfaces, the (1 × 1) structures are shown in Fig. 1 and will be used in all following discussion.

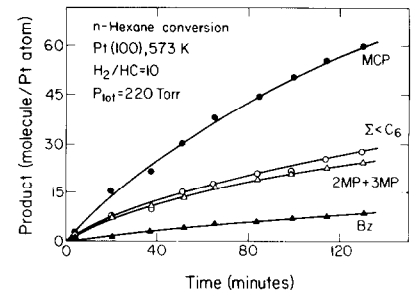

FIG. 2. Product accumulation curves measured as a function of reaction time at 573 K for *n*-hexane conversion over Pt(100).

3. RESULTS

Structure sensitivity of catalyzed n-hexane reactions. Product accumulation curves determined as a function of reaction time at 573 K (H_2/HC = 10) for *n*-hexane reactions catalyzed on the (100) platinum surface are shown in Fig. 2. Product accumulation curves determined at 573 K (H_2/HC = 10) for aromatization catalyzed over four platinum surfaces are compared in Fig. 3. The rate of reaction at any time is given

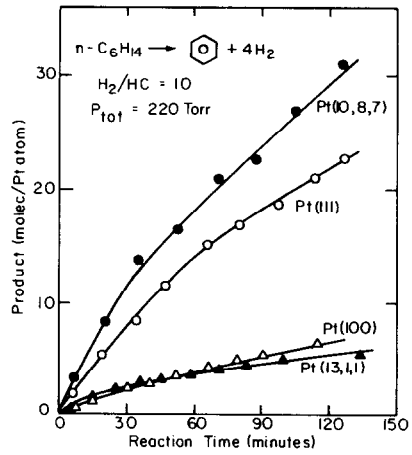

FIG. 3. Product accumulation curves measured as a function of reaction time at 573 K for *n*-hexane aromatization catalyzed over platinum single crystal surfaces.

TABLE 2

Initial Reaction Rates, Selectivities, and Surface Carbon Coverages for *n*-Hexane Reactions Catalyzed Over Platinum Single Crystal Surfaces[a]

Catalyst	Initial reaction rates (molec/Pt atom s) × 10^{3}[b]				Selectivities[c] (mol %)			Surface carbon[d]
	$\Sigma < C_6$	2MP + 3MP	MCP	Bz	S_{isom}	$S_{cyc.}$	S_{hydr}	
Pt(100)	5.7	6.8	9.8	1.4	29	47	24	2.3
Pt(13,1,1)	6.8	4.3	9.5	1.6	19	50	31	2.5
Pt(111)	8.7	7.9	11	4.9	24	50	26	2.2
Pt(332)	8.0	3.0	11	4.5	12	58	30	2.2
Pt(10,8,7)	6.4	6.0	12	6.0	20	59	21	2.0
Approximate activation energies (kcal/mol)[e]								
P_{H_2} = 200 Torr		20–25		16–22		13–19		23–28
P_{H_2} = 600 Torr		22–26		~25		19–25		26–32

[a] At 573 K, H_2/HC = 10, P_{tot} = 220 Torr.
[b] ±25%.
[c] Fractional selectivities; isom = 2MP + 3MP, cyc = MCP + Bz, hydr = $\Sigma < C_6$.
[d] Carbon atoms per surface Pt atom at 110–150 min.
[e] Average spread in values for different surfaces at 550–580 K.

by the slope of the product accumulation curve at that time. Table 2 summarizes initial reaction rates and selectivities at 573 K for the different reaction pathways together with surface carbon coverages that were determined by AES following 110–170 min reaction time. Only the aromatization reaction displayed significant structure sensitivity that was characterized by about a factor of 4 difference in initial rates between the most active (10,8,7) and least active (100) platinum surfaces. All other reactions displayed initial rates that differed by less than a factor of 2 on all the platinum surfaces.

Temperature and pressure dependence of the initial reaction rates. Arrhenius plots for *n*-hexane hydrogenolysis, isomerization, C_5-cyclization, and aromatization catalyzed over five platinum surfaces at a total pressure of 220 Torr are shown in Figs. 4–7. The (10,8,7) (332), and (111) platinum surfaces were always more active in aromatization as compared to the (13,1,1) and (100) surfaces. All other reactions displayed little structure sensitivity at all reaction temperatures.

Hydrogenolysis and aromatization were the only reactions that displayed "normal" Arrhenius behavior over a wide range of temperature. Even for these reactions the apparent activation energies appeared to decrease with increasing reaction temperature. Since the initial rates in the Arrhenius plots refer to reactions on clean platinum surfaces, it is possible that the behavior at high temperature is due to competition between the *n*-hexane conversion and the de-

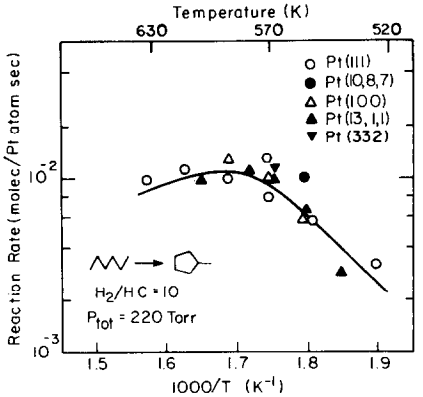

FIG. 4. Arrhenius plot for *n*-hexane cyclization to methylcyclopentane catalyzed over platinum single crystal surfaces.

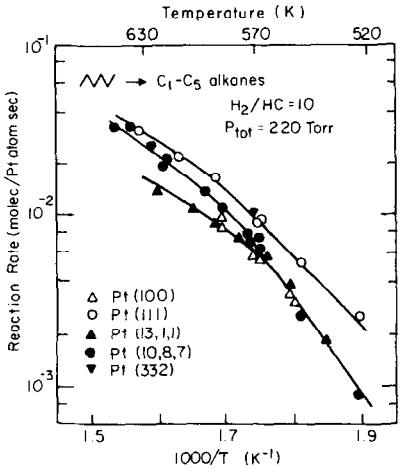

FIG. 5. Arrhenius plots for *n*-hexane hydrogenolysis catalyzed over platinum single crystal surfaces.

activation of the catalyst by the formation of carbonaceous deposits. The role of these deposits will be discussed later. The isomerization and C_5-cyclization reactions displayed rate maxima at temperatures that varied from about 570 K for 2MP formation

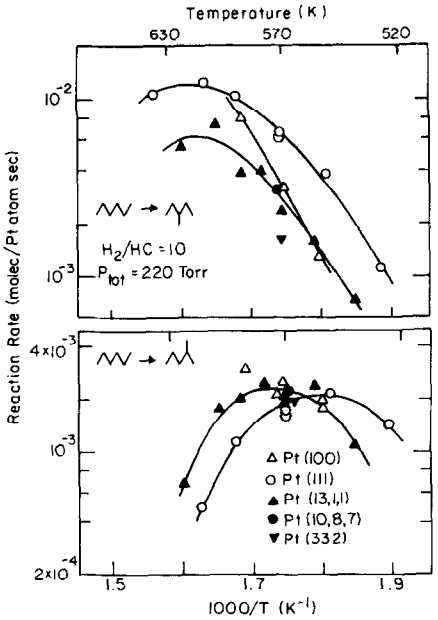

FIG. 6. Arrhenius plots for *n*-hexane isomerization to 2-methylpentane (below) and 3-methylpentane (above) catalyzed over platinum single crystal surfaces.

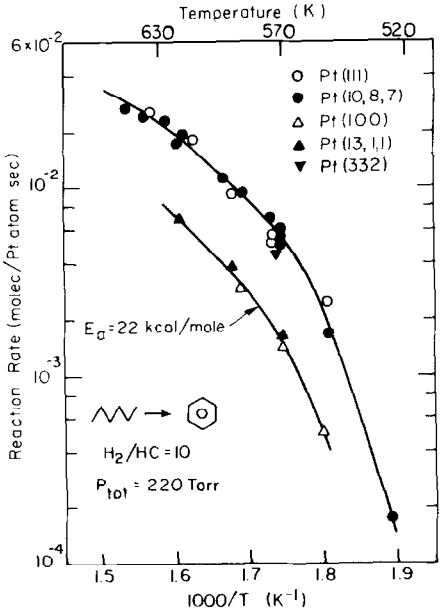

FIG. 7. Arrhenius plots for *n*-hexane aromatization catalyzed over platinum single crystal surfaces.

to 600–620 K for 3MP and MCP production. Figure 8 shows Arrhenius curves plotted together for all the parallel reactions catalyzed on the (13,1,1) platinum surface at a total pressure of 220 Torr. Similar results were obtained with the (111) and (10,8,7) platinum surfaces at a total pressure of 620 Torr as shown for Pt(10,8,7) in Fig. 9. Over these surfaces the rate maxima

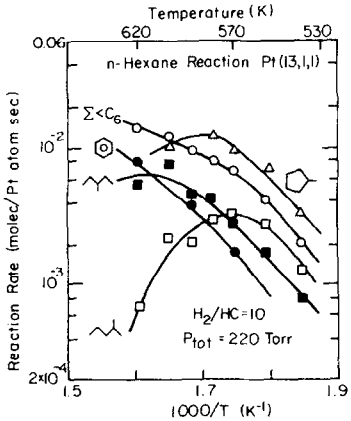

FIG. 8. Arrhenius plots for *n*-hexane reactions catalyzed over the stepped (13,1,1) platinum surface (H_2/HC = 10; P_{tot} = 220 Torr).

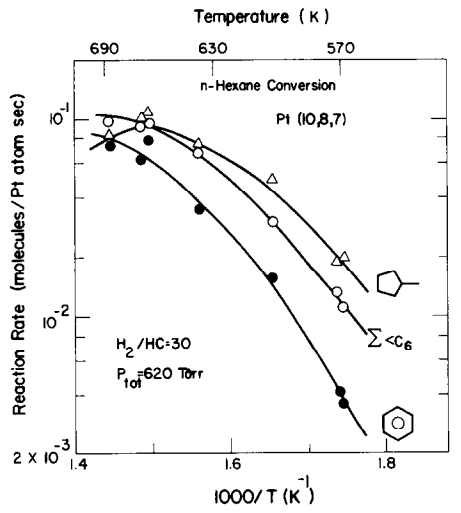

FIG. 9. Arrhenius plots for *n*-hexane reactions catalyzed over the kinked (10,8,7) platinum surface (H_2/HC = 30, P_{tot} = 620 Torr).

appeared to shift to higher temperatures with increasing hydrogen pressure.

The unusual temperature dependencies observed for the *n*-hexane reactions (coupled with more rapid deactivation at high temperatures) prevented a reliable determination of activation energies for temperatures higher than about 600 K. Table 2 includes average apparent activation energies at two total pressures that were estimated from the Arrhenius plots for reaction temperatures of 560–590 K. Based on the limited data at these lower temperatures, these activation energies are believed to be accurate to no more than ±5 kcal/mol. Nevertheless, a clear tendency existed for the apparent activation energies to increase with increasing hydrogen pressure.

Reaction order plots for *n*-hexane hydrogenolysis and aromatization catalyzed over the kinked (10,8,7) platinum surface are shown at several temperatures in Fig. 10. The order of the hydrogenolysis reaction with respect to hydrogen pressure appeared to increase from about 0.4 at 573 K to 0.9 at 640 K. Isomerization and C_5-cyclization displayed similar behavior (at 573 K). The order of the aromatization reactions with respect to hydrogen pressure was slightly negative at low temperatures (<590 K) but became positive at higher temperatures (>590 K).

Reaction selectivity. Because parallel reactions displayed different catalytic behavior as a function of temperature and hydrogen pressure, the selectivities for *n*-hexane conversion over the single crystal catalysts varied markedly with reaction conditions. Fractional selectivities for *n*-hexane hydrogenolysis, dehydrocyclization (MCP + Bz), and isomerization (2MP + 3MP) catalyzed over Pt(111) at a total pressure of 620 Torr are shown as a function of reaction temperature in the upper half of Fig. 11. Kinetic selectivities for the production of 2MP over 3MP and Bz over MCP are shown as a function of temperature in the lower half of Fig. 11. Figure 12 illustrates the same kinetic selectivity functions for *n*-hexane reactions catalyzed over five platinum surfaces at a total pressure of 220 Torr. The 2MP/3MP ratios always decreased and the Bz/MCP ratios always increased with increasing reaction temperature. The temperature ranges where these selectivities changed most rapidly shifted toward higher temperatures with increasing hydrogen pressure.

Hydrogenolysis selectivities. Whereas the catalytic activity for *n*-hexane hydrogenolysis displayed little dependence on

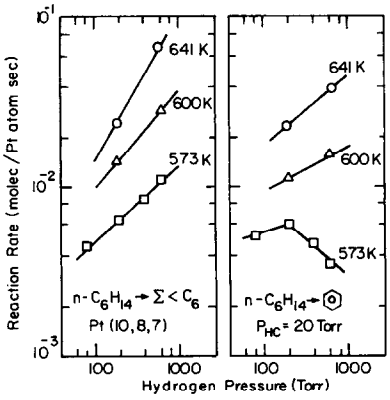

FIG. 10. Order plots at 573–641 K for Pt(10,8,7) showing the dependence of *n*-hexane hydrogenolysis and aromatization rates on hydrogen pressure (P_{HC} = 20 Torr).

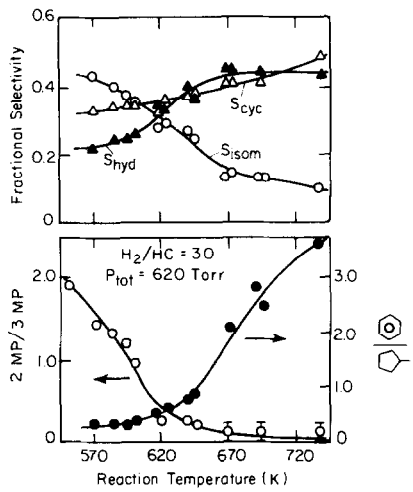

FIG. 11. Temperature dependence of the initial selectivities for *n*-hexane reactions catalyzed over Pt(111) (H_2/HC = 30, P_{tot} = 620 Torr): fractional selectivities for hydrogenolysis, isomerization (2MP + 3MP), and cyclization (MCP + Bz) are shown above; kinetic selectivities for 2MP/3MP and Bz/MCP are shown below.

platinum surface structure, the selectivity during hydrogenolysis varied markedly with terrace structure and, to a lesser extent, with hydrogen pressure. Product distributions for *n*-hexane hydrogenolysis catalyzed over the platinum surfaces are summarized for a variety of reaction conditions in Table 3. The (100) and (13,1,1) platinum surfaces displayed a clear preference for scission of internal C–C bonds leading primarily to the formation of ethane, propane, and butane. By contrast the (111), (332), and (10,8,7) platinum surfaces displayed high selectivities for cleavage of the terminal and central C–C bonds. Low levels of multiple hydrogenolysis (n-$C_6H_{14} \rightarrow CH_4 + C_2H_6$) that represented about 3–8% of the total C–C bond breaking activity at 573 K, were detected over all the platinum surfaces. Multiple C–C bond breaking processes were favored at high reaction temperatures and appeared to occur most easily on the (111), (332), and (10,8,7) platinum surfaces.

The fission parameter, M_f, defined by (*17*):

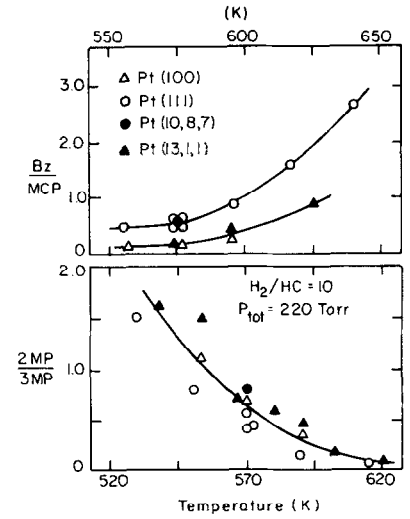

FIG. 12. Temperature dependence of the initial kinetic selectivities for Bz/MCP (above) and 2MP/3MP (below) determined for *n*-hexane reactions catalyzed over platinum single crystal surfaces (H_2/HC = 10, P_{tot} = 220 Torr).

TABLE 3

Initial Product Distributions for *n*-Hexane Hydrogenolysis Catalyzed over Platinum Single Crystal Surfaces[a]

Catalyst	T (K)	P_{H_2} (Torr)	Initial hydrogenolysis Distributions (mol)				
			C_1	C_2	C_3	C_4	C_5
Pt(100)	556	220	13	20	42	18	7
	573	200	16	19	39	19	7
	592	200	18	20	38	16	8
Pt(111)	573	200	31	11	32	8	18
	593	200	36	10	30	5	19
	638	200	43	16	24	4	13
Pt(13,1,1)	573	200	15	22	39	17	7
	595	200	15	23	40	16	6
	623	200	16	22	43	13	6
Pt(10,8,7)	573	200	36	13	27	12	12
	599	200	30	10	37	10	13
	623	200	33	12	36	9	10
	658	200	36	14	31	10	9
Pt(332)	573	200	43	13	20	10	13
Pt(111)	573	600	23	14	35	12	16
	623	600	28	15	33	8	16
	673	600	40	15	24	6	15
	753	600	64	13	14	2	7
Pt(10,8,7)	573	80	37	14	28	11	10
	573	600	31	17	24	14	14

[a] Product distributions were calculated at 15–30 min reaction time, P_{HC} = 20 Torr.

$$M_f = [C_1]^{-1} \sum_{i=2}^{5} (6 - i)[C_i] \qquad (1)$$

was used to classify the hydrogenolysis selectivities that were exhibited by the different platinum surfaces. The concentrations of hydrogenolysis products with i carbon atoms are denoted by $[C_i]$. Selective hydrogenolysis of the terminal C–C bond produces $M_f = 1$, whereas purely statistical hydrogenolysis yields $M_f = 10$. When multiple hydrogenolysis is important, $M_f < 1$. Fission parameters for n-hexane hydrogenolysis catalyzed at a total pressure of 220 Torr are shown as a function of reaction temperature in Fig. 13. The (111), (332), and (10,8,7) platinum surfaces displayed values of M_f that were between 3 and 7 for all temperatures between 530 and 660 K. Fission parameters for the (100) and (13,1,1) surfaces were always much higher, i.e., 13–21. The fission parameters displayed a small dependence on hydrogen pressure, as shown for the (111) platinum surface in Fig. 14. High hydrogen partial pressures and low temperatures favored statistical hydrogenolysis, whereas low hydrogen pressures and high temperatures favored terminal C–C bond splitting.

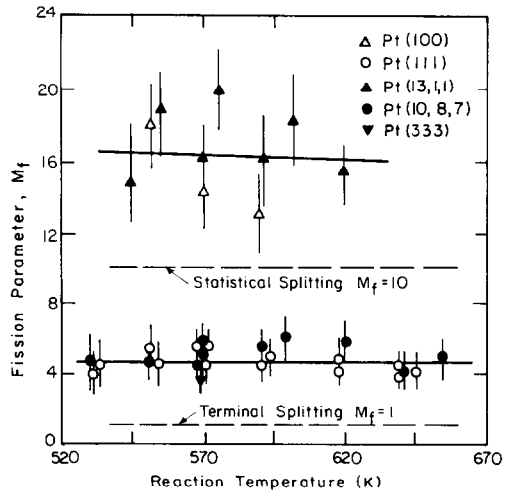

FIG. 13. Fission parameters determined as a function of reaction temperature for n-hexane hydrogenolysis catalyzed over platinum single crystal surfaces (H_2/HC = 10, P_{tot} = 220 Torr).

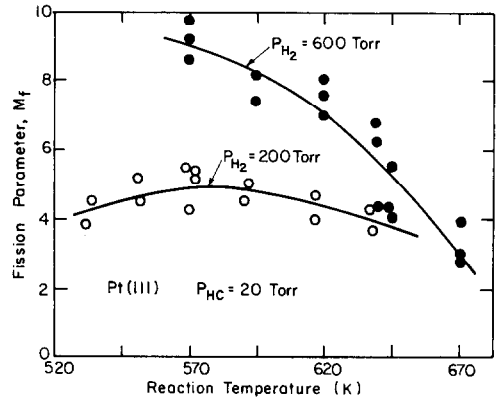

FIG. 14. Fission parameters determined as a function of reaction temperature for n-hexane hydrogenolysis catalyzed over Pt(111) showing the dependence of hydrogenolysis selectivity on hydrogen pressure (P_{HC} = 20 Torr).

Deactivation kinetics and formation of surface carbon deposits. Continuous deactivation was detected during all the n-hexane reaction studies. Parallel reactions displayed similar deactivation rates under each set of reaction conditions. However, within isomerization, the deactivation behavior 2- and 3-methylpentane formation was clearly different. The selectivity for 2-methylpentane production relative to 3-methylpentane formation increased with increasing reaction time. This effect was most pronounced for the (100) and (13,1,1) platinum surfaces, where a two- to threefold change in selectivity was detected after 2–3 h (*38*).

Deactivation rates at any given temperature were similar for all platinum surfaces. The deactivation rates increased with increasing reaction and decreasing hydrogen pressure. Deactivation resulted from the formation of strongly adsorbed, partially dehydrogenated, carbonaceous deposits that covered a significant fraction of the platinum surface (*32*). Figure 15 compares AES spectra recorded following n-hexane reaction studies over Pt(100) at 573 and 673 K. As indicated, the surface coverage by the carbonaceous deposit increased with in-

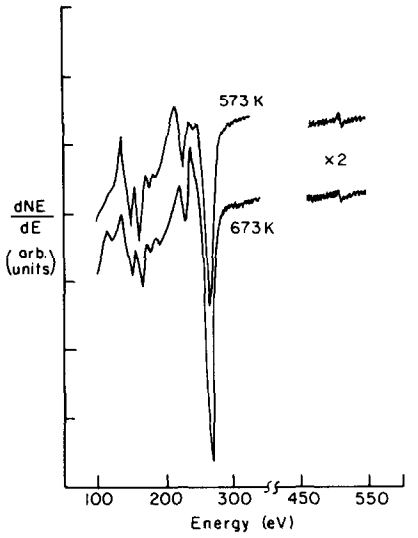

FIG. 15. Auger spectra recorded after *n*-hexane reaction studies catalyzed over Pt(100) at 573 and 673 K.

creasing reaction temperature. Figure 16 summarizes C_{273}/Pt_{237} AES peak-to-peak height ratios measured following *n*-hexane reactions that were carried out between 525 and 678 K. These peak height ratios can be converted into approximate atomic ratios expressed as carbon atom equivalents per surface platinum atom by multiplying by 0.62 for Pt(111), (332), and Pt(10,8,7), and by 0.74 for Pt(100) and Pt(13,1,1), respectively (*39*). Using these conversions, it follows that the apparent coverage by the deposit was equivalent to 1–6 carbon atoms per surface platinum atom.

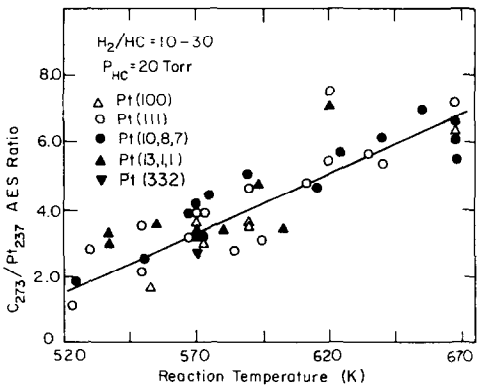

FIG. 16. Temperature dependence of the C_{273}/Pt_{237} AES peak-to-peak height ratio measured following *n*-hexane reaction studies on platinum single crystal surfaces.

Several different kinetic models were investigated to describe the deactivation kinetics. At the lowest temperatures investigated (<560 K), the deactivation was well described by a first-order model, $R_t = R_0 \exp(-\alpha t)$, whereas at higher temperatures the deactivation displayed a fractional order time dependence; viz., $R_t = R_0 \exp(-\alpha t^n)$, $0 < n \leq 1$. Best fit orders for the deactivation process were determined from order plots (not shown) of $\ln(\ln(R(t)/R_0))$ as a function of $\ln t$. Deactivation orders determined in this manner decreased continuously with increasing reaction temperature from 1.0 ± 0.2 at 520–570 K to 0.5 ± 0.2 at 640–660 K. The apparent activation energy for deactivation was estimated from the initial slopes of plots testing the first and half-order deactivation models. Arrhenius plots for the deactivation rate constants yielded activation energies that were always in the range 11–18 kcal/mol independent of the deactivation model (*39*).

n-Hexane dehydrogenation activity. The dehydrogenation of *n*-hexane yielded an unresolved mixture of 1-, *cis*- and *trans*-2-, and *cis*- and *trans*-3-hexenes under all reaction conditions. The dehydrogenation reactions were very rapid and approached equilibrium over the first 20–30 min reaction time. Hexenes detected in the first gas chromatogram of each experiment were used to establish a lower limit for the initial dehydrogenation rates. These "lower limit" dehydrogenation rates are shown as a function of $1/T$ in Fig. 17. The dehydrogenation rates estimated in this manner (in the range 0.1–1 molec/Pt atom s) were at least 10 times faster than the sum rate of all skeletal rearrangement reactions.

4. DISCUSSION

Structure sensitivities of initial n-hexane reaction rates. Important new information about the structure sensitivities of alkane reforming reactions have been derived from

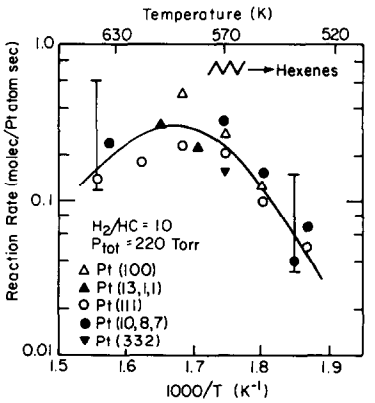

FIG. 17. Arrhenius plot for *n*-hexane dehydrogenation catalyzed over platinum single crystal surfaces (H_2/HC = 10, P_{tot} = 220 Torr). The initial rates shown are lower limits to the absolute rates which could not be accurately determined due to thermodynamic constraints.

our studies of *n*-hexane reactions catalyzed over platinum single crystal surfaces. Near atmospheric pressure and temperatures between 550 and 620 K, the (111), (332), and (10,8,7) platinum surfaces were several times more active than the (100) and (13,1,1) surfaces for the dehydrocyclization of *n*-hexane to benzene. Hexagonal (111) microfacets that were present in highest concentrations on the (111), (332), and (10,8,7) surfaces displayed a unique ability to catalyze this complex skeletal rearrangement. The atomic structure of the terraces was the major source of structure sensitivity for this important reforming reaction. Steps and kinks that were present in high concentrations on the (13,1,1) and (10,8,7) surfaces increased the rate of dehydrocyclization only 10–40% as compared to the flat low index surfaces. It should be noted that unoriented crystal edges that represented ~8–15% of the total platinum surface area tend to make the structure sensitivities appear smaller than they would be if the entire platinum surface area were of the specified orientation.

In contrast to aromatization, the rates of *n*-hexane hydrogenolysis, isomerization, and C_5-cyclization displayed little dependence on platinum surface structure. The absence of significant structure sensitivity for these reactions is consistent with the studies of Ponec *et al.* (*5*) (Pt/SiO_2, H_2/HC = 16, P_{tot} = 1 atm, T = 520–570 K) and Dautzenberg and Platteeuw (*7, 8*) (Pt/Al_2O_3, H_2/HC = 4, P_{tot} = 9.5 atm, 760 K). An important result of our studies is that C_5-cyclization occurred very easily on all the platinum surfaces, even the flat (111) and (100) surfaces with very low concentrations of step and kink defect sites. At the lower temperatures (530–570 K), methylcyclopentane was the dominant reaction product produced over every surface. It has often been suggested that isolated edge and corner atoms are the preferred sites for this C_5-cyclization reaction (*5, 25, 40, 41*). Our studies demonstrate that under appropriate conditions all types of platinum sites can catalyze this pathway with high selectivity.

It appears likely that corner atoms with very few (3 or 4) nearest neighbors and/or metal support interactions may be responsible for the exceptional C_5-cyclization selectivity that has often been reported for supported platinum catalysts with very high dispersion (*5, 22, 25, 41*).

In Fig. 18 the initial rates of aromatization and C_5-cyclization at 573 K are summarized as a function of surface structure. Aromatization was influenced strongly by the terrace structure, whereas C_5-cyclization was not. Terraces with (111) orientation led to a higher aromatization specificity. Further studies using more highly stepped and kinked surfaces would be valuable to further extend this conclusion.

Isomerization of *n*-hexane to 2- and 3-methylpentanes displayed little if any structure sensitivity. All types of platinum sites were highly active for catalyzing this skeletal rearrangement process, although the flat (111) surface appeared to be slightly more active than the other platinum surfaces, especially for the production of 3-methylpentane.

The structure sensitivities of *n*-hexane reactions reported here compare favorably

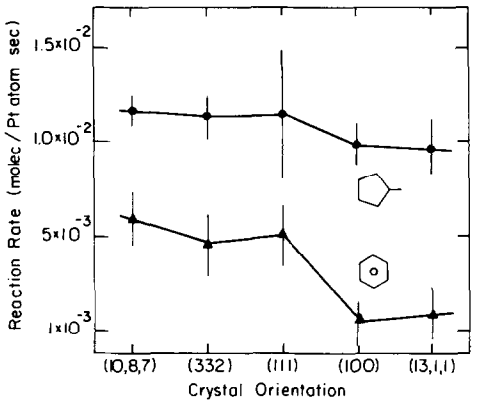

FIG. 18. Structure dependence of *n*-hexane C_5-cyclization and aromatization rates on platinum single crystal surfaces with different crystallographic orientation (at 573 K, H_2/HC = 10, P_{tot} = 220 Torr).

with results recently obtained by Gillespie for *n*-heptane hydrogenolysis and aromatization catalyzed over flat (111), stepped (557), and kinked (25,10,7), and (10,8,7) platinum surfaces (*29*). As compared to the flat (111) surface, *n*-heptane aromatization was faster and hydrogenolysis was slower by about a factor of 2 on the kinked (10,8,7) surface. The same trend was detected for *n*-hexane reactions, although the differences in rates due to surface irregularities were less pronounced.

Finally, it should be noted the overall *n*-hexane skeletal rearrangement rates determined for single crystal surfaces were always much higher than the rates of the same reactions catalyzed over practical platinum catalysts. Table 4 provides a comparison of initial rates for Pt(111) with those reported for other types of platinum catalysts, e.g., film, powders, and Pt/SiO_2. All the rates were determined under similar reaction conditions. With the exception of ultra thin platinum films that were prepared in UHV (*4*), the initial rates for Pt(111) were usually about an order of magnitude higher than rates reported for practical catalysts. As noted by Gillespie (*29*) these differences probably arise from a combination of effects including (a) metal support interactions, (b) carbonaceous deposits on the practical catalysts, and (c) inaccuracies in surface area determinations for the model and/or practical catalysts. In any case, with the single crystal platinum the activity decreases with time, due to the poisoning by the carbonaceous deposits, and after a few hours it reaches a value comparable to that of the supported catalysts.

n-Hexane reaction selectivity. Product distributions for *n*-hexane skeletal rearrangement over the single crystal catalysts displayed striking variations as a function of temperature and hydrogen pressure. For any set of reaction conditions the product distributions for all surfaces were similar except for the differences in aromatization selectivity that are expected from the structure sensitivity of this reaction. Isomerization, C_5-cyclization, and hydrogenolysis were always the main reactions at lower temperatures (≤570 K) and higher hydrogen pressures (≥200 Torr). Hydrogenolysis and aromatization selectivities increased with increasing temperature. At the highest temperatures studied (≥620 K) hydrogenolysis and aromatization represented 65–90% of the total skeletal rearrangement.

Product distributions determined at the lower reaction temperatures (530–590 K) were generally very similar to those reported previously for supported catalysts, as indicated in Table 5, where a detailed comparison is provided with other types of

TABLE 4

Comparison of Initial *n*-Hexane Reaction Rates on Pt(111) and Practical Platinum Catalysts

Catalyst	*T* (K)	H_2/HC	P_{tot} (Torr)	Initial rate[a] (molec/Pt atom s)	Ref.
Pt(111)	573	10	220	0.03	—
Pt-powder	573	6	760	3×10^{-3}	(*2*)
Pt/SiO_2 ($\bar{d}$ = 30 Å)	573	11.2	180	4×10^{-4}	(*10*)
Pt(111)	553	10	220	0.02	—
Pt-film ($\bar{d}$ = 15–58 Å)	546	10	110	0.02–0.03	(*4*)
Pt(111)	573	30	620	0.07	—
Pt/SiO_2 ($\bar{d}$ = 40–80 Å)	573	16	750	$3–4 \times 10^{-3}$	(*5*)

[a] Total rate of skeletal rearrangement.

TABLE 5

Comparison of *n*-Hexane Reaction Selectivities for Single Crystal Surfaces and Practical Platinum Catalysts

Catalyst	T (K)	H_2/HC	P_{tot} (Torr)	Fractional selectivities (mol %)				2MP/3MP	Bz/MCP	Ref.
				2MP + 3MP	MCP	Bz	$\Sigma < C_6$			
Pt/Al_2O_3	573	190	760	58	7.5	2	32.5	1.5	0.27	(*16*)
16% Pt/SiO_2	567	17	760	48	7	2	43	1.7	0.29	(*14*)
0.22% Pt/SiO_2 ($\bar{d}$ = 10 Å)	573	~11	760	29	35	—	36	2.8	—	(*6*)
9.5% Pt/SiO_2 ($\bar{d}$ = 55 Å)	573	~11	760	53	7	—	40	2.6	—	(*6*)
Pt-black	573	6	760	49	10	1–3	38	—	≤0.3	(*2*)
Pt(111)	573	30	620	42	26	7	25	1.5	0.27	—
1% Pt/SiO_2 ($\bar{d}$ = 30 Å)	573	13.5	190	71	2.5	0.5	26	—	0.2	(*10*)
Pt(111)	573	10	220	24	35	15	26	0.4	0.6	—
Pt(100)	573	10	220	29	41	6	24	0.65	0.14	—
1% Pt/SiO_2 (d = 30 Å)	635	13.5	190	56	18	4	22	—	0.22	(*10*)
Pt(111)	638	10	220	14	13	33	40	≤0.15	2.6	—
Pt-black	693	>20	760	5	4	18	73	—	5.0	(*3*)
Pt(111)	693	30	620	14	11	32	43	<0.2	2.8	—

platinum catalysts. In nearly all cases the single crystal surfaces displayed higher selectivities for aromatization and C_5-cyclization and lower selectivities for isomerization as compared to practical catalysts. However, these selectivity differences were small enough that the overall agreement must be considered very good.

One would hope to be able to decompose the selectivities displayed by practical catalysts as a linear combination of selectivities for (100) and (111) microfacets. Unfortunately this is not possible because the cyclization selectivities displayed by single crystal surfaces are always too high.

Kinetic selectivities for 3MP over 2MP and Bz over MCP increased markedly with increasing temperature and decreasing hydrogen pressure. These changes in selectivity were quite dramatic indicating that major changes occurred in the reaction mechanism as a function of reaction conditions. The 2MP/3MP and Bz/MCP selectivities determined at lower temperatures (<570 K) and higher hydrogen pressures (H_2/HC ≥ 30) were similar to these noted previously for practical catalysts. However, the very low 2MP/3MP ratios (≤0.2) and very high Bz/MCP ratios (≥2–3) determined at higher temperatures and lower hydrogen pressures appear to be unique to single crystal surfaces and perhaps other forms of bulk platinum. In studies of *n*-hexane reactions catalyzed over Pt/SiO_2 catalysts, van Schaik *et al.* (*14*) and Karpinski and Koscielski (*10*) failed to observe significant changes in the same kinetic selectivities over the temperature ranges 550–585 and 573–635 K, respectively. At high space velocities, 9.5 atm (H_2/HC = 4), and 710–760 K, 2MP/3MP and Bz/MCP ratios of about 2 and 0.1–0.5, respectively, were reported for monofunctional Pt/Al_2O_3 catalysts (7.8). Paal has reported Bz/MCP ratios as large as 5 for *n*-hexane reactions catalyzed over Pt-black at 690 K (*3*).

Maire and co-workers (*41*) recently investigated the isomerization of 2-methylpentane-2-^{13}C on several platinum single crystal surfaces and on a series of alumina supported platinum catalysts. The isotopic distribution of ^{13}C in the product hexanes was used to determine the proportion of the isomerization reaction which proceeded by the C_5-cyclic mechanism. At 620–720 K, the (111), (911), and (557) single crystal catalysts displayed cyclic percentages which were in the range 14–70%, although most

often they were 50–70%. Since these cyclic percentages were the same as those displayed by supported catalysts with low and medium dispersion (<0.7), the Strasbourg group concluded that the single crystal surfaces are excellent models of practical catalysts with low and medium dispersion. While meaningful labeling studies could not be carried out under our low conversion conditions, two facts certainly tend to demonstrate that *the cyclic mechanism is important on the single crystal surfaces.* Isomerization and C_5-cyclization displayed identical catalytic behavior as a function of temperature and hydrogen pressure; both reactions displayed maximum rates at 600–630 K, and both reactions displayed similar absolute rates over all surfaces under all conditions investigated. More importantly, whereas *n*-hexane isomerization exhibited no significant structure sensitivity, isobutane and *n*-butane isomerization were highly structure sensitive over the same platinum surfaces under exactly the same reaction conditions used for the *n*-hexane reactions studies (*31*). These light alkanes are restricted to isomerization by the bond shift mechanism which is fastest on surfaces containing mostly (100) surface structure. It is difficult to rationalize a process by which bond-shift isomerization would be structure sensitive for isobutane and *n*-butane but not *n*-hexane, unless, of course, the bond-shift pathway is of lesser importance for *n*-hexane.

If it is accepted that *n*-hexane isomerization is at least partially cyclic, then the changes in 2MP/3MP selectivity with temperature, hydrogen pressure, and reaction time could result from changes in the positional selectivity for ring opening of the C_5-cyclic intermediates. Isomerization to 3-methylpentane was favored in initially clean platinum at high temperatures and low hydrogen pressures. Isomerization to 2-methylpentane was favored at longer reaction times after the surfaces had become extensively covered by strongly adsorbed carbonaceous species. Similar changes in isomerization selectivity with reaction time were noted by Carra *et al.* (*2*) for *n*-hexane conversion at 573 K over platinum black and also for methylcyclopentane ring opening over platinum single crystal model catalysts (*38*). It appears likely that this change in selectivity as carbon is deposited on the surface may arise from a change in the steady state surface concentration of chemisorbed hydrogen and/or a change in the size of the available reaction sites (*32*).

The results obtained in this work demonstrate that direct 1,6-ring closure is an important reaction pathway for *n*-hexane aromatization on platinum. Aromatization was structure sensitive and favored by high temperatures and low hydrogen pressures. By contrast C_5-cyclization was structure insensitive with maximum selectivity at lower temperatures (<570 K) and higher hydrogen pressures (H_2/HC > 10). These differences in catalytic behavior appear to indicate that the reaction intermediates leading to aromatization have a lower hydrogen content than those leading to methylcyclopentane formation. With this in mind, it is possible that the structure sensitivity of n-hexane aromatization may originate in part from the different binding strengths of hydrogen on the surfaces with different atomic structure. It is well established that hydrogen is chemisorbed more strongly on (100) microfacets than (111) microfacets by about 1–4 kcal/mol (*42–44*). The steady state concentration of surface hydrogen should therefore be higher on surfaces with (100) terraces. An increase in the concentration of surface hydrogen would be accompanied by a decrease in the concentration of reaction intermediates with very low hydrogen content (all other things being equal). As a result, it is natural to expect that the aromatization activity of (100) microfacets should be lower than that for (111) microfacets. Differences in aromatization rate constants that arise directly from changes in surface structure (template effect) might also contribute to the unique

structure sensitivity of the aromatization reaction.

Hydrogenolysis product distributions. The positional selectivity of *n*-hexane hydrogenolysis displayed a marked dependence on platinum surface structure. The (100) and (13,1,1) platinum surfaces with high concentrations of (100) microfacets displayed a high specificity for scission of the internal C–C bonds with little accompanying terminal hydrogenolysis ($M_f \gtrsim 15$). By contrast, the (111), (332), and (10,8,7) surfaces that were mostly composed of hexagonal (111) microfacets displayed a clear preference of hydrogenolysis of the central and terminal C–C bonds. In this case, the probability for scission of the C_2–C_3 bond was quite low. Average C–C bond rupture probabilities calculated for Pt(100) and Pt(111) at a total pressure of 220 Torr were

	C_1–C_2	C_2–C_3	C_3–C_4	C_4–C_5	C_5–C_6
Pt(100)	0.08	0.20	0.44	0.20	0.08
Pt(111)	0.21	0.09	0.40	0.09	0.21

These probabilities differ appreciably from those reported previously for supported platinum catalysts where *n*-hexane hydrogenolysis was most often statistical (*4, 6, 10*), although in a few cases (*14, 16*) a small preference was reported for internal scission (like Pt(100)).

The differences in hydrogenolysis selectivity for single crystal surfaces with different atomic structure appear to arise directly from differences in the structure of the reaction intermediates which undergo C–C bond scission. Existing literature (*26, 27, 45, 46*), suggests that α,γ-triadsorbed species are the most important class of intermediates for hydrogenolysis reactions of C_3 and larger alkane molecules. Convincing evidence in favor of these species was provided by Leclercq and co-workers (*47*) in studies of sixteen different alkane hydrogenolysis reactions catalyzed over Pt/Al_2O_3. In that case, the reactivities of C–C bonds with different substitution were always well described by the intervention of 1,1,3- and 1,3,3-triadsorbed species, except when the carbon-3 was quarternary, in which case α,δ-adsorbed species also appeared to become important. The French workers also presented evidence that hydrogenolysis was most favorable for C–C bonds α to a metal–carbon multiple bond. The latter prediction is consistent with recent extended Huckel calculations (*48*) which revealed that C–C bonds α to platinum–carbon multiple bonds in alkylidene ($Pt = CR_2$) and alkylidyne ($Pt \equiv CR$, $R = CH_3$) surface species are weakened relative to those α to platinum–carbon single bonds (*49*).

In addition to these α,γ-triadsorbed species, another possibility, which is clearly unique to (111) microfacets, can be proposed to account for the higher selectivities for terminal cleavage on surfaces containing these structures. Dynamical LEED intensity analysis and high resolution ELS studies (*50–54*) have demonstrated that a common, stable surface species always results from the chemisorption of ethylene, propylene, and butenes on Pt(111), Pd(111), and Rh(111) at 300–420 K. This species is the surface alkylidyne group, $Pt_3 \equiv C–R$ ($R = CH_3$, C_2H_5, C_3H_8), which occupies the threefold hollow sites that are unique to (111) microfacets. Atomic structures for these species chemisorbed on Pt(111) are shown in Fig. 19 (*54*). Formation of these surface species is accompanied by weakening of the α-C–C bond (*48*). If the isostructural hexylidyne species formed during *n*-hexane conversion on the (111) platinum surface, hydrogenolysis should yield methane and pentane with high selectivity as observed experimentally.

Deactivation kinetics and role of adsorbed carbonaceous deposits. The platinum single crystal catalysts deactivated continuously during all of the *n*-hexane reaction studies. The deactivation rate displayed little dependence on platinum surface structure. Deactivation was accompanied by the deposition of about

one or more monolayers of disordered, strongly bound carbonaceous deposit on the platinum surfaces that could be detected following the reactions by AES. The deactivation kinetics could be described empirically by an exponential rate law, $R(t) = R(t = 0) \exp(-\alpha t^n)$, where the order parameter n decreased with increasing reaction temperature. In order to place these deactivation kinetics in context, three important properties of the carbon deposit that were discussed previously (*32*) should be considered: (i) the carbonaceous deposit is a nongraphitic, polymeric residue with an average hydrogen content of about one hydrogen atom per surface carbon atom, (ii) the carbonaceous deposit nucleates in the form of islands that are largely two-dimensional at low temperatures (<570 K) but tend to become three-dimensional at high temperatures (>630 K), and (iii) the general role of the carbon deposit is that of a nonselective poison; in its presence hydrocarbon catalysis takes place on a small concentration of uncovered surface platinum ensembles that display normal platinum activity and selectivity.

A simplified kinetic model for the deactivation process can be developed from the following series of reaction steps

$$n\text{-}C_6H_{14} \overset{\lambda}{\rightleftharpoons} n\text{-}C_6H_x(\text{ads}) + aH_2 \quad \begin{matrix} \xrightarrow{k_p} \text{carbon deposit} \\ \xrightarrow{} \text{products} \end{matrix} \tag{2}$$

where it is proposed that deactivation results from polymerization of adsorbed reactant molecules. According to this scheme hydrocarbon conversion competes with deactivation, and dissociative hydrocarbon chemisorption is reversible as demonstrated by recent deuterium exchange studies (*34*). The rate of skeletal rearrangement is proportional to $k_r\theta_i$ where θ_i is the surface coverage by adsorbed hydrocarbon. This θ_i does not include any assumptions on the ensemble size requirements for the different reactions. Since the deactivation rate was slow compared with the individual adsorption–desorption and surface reaction steps (*34*), the steady state approximation can be applied to θ_i which yields

$$\theta_i = \frac{\lambda P_{HC}(1 - \theta_c)}{(\lambda P_{HC} + K_H{}^a P_{H_2}{}^a + k_r/k_{-1} + k_p/k_{-1})} = \eta(1 - \theta_c) \tag{3}$$

where $\lambda = k_1/k_{-1}$, θ_c is the surface coverage by the deactivating carbon deposit, and the surface coverage by hydrogen is assumed to be small for simplicity (i.e., $\theta_H \ll (K_H P_{H_2})^{1/2}$). The rate of formation of this deposit is simply

$$\frac{d\theta_c}{dt} = k_p\theta_i = \eta k_p(1 - \theta_c) \tag{4}$$

which integrates to

$$\theta_i(t) \approx \exp(-\eta k_p t) \tag{5}$$

The latter expression accounts for the first-order deactivation that was observed at lower temperatures and predicts that the deactivation rates should increase with in-

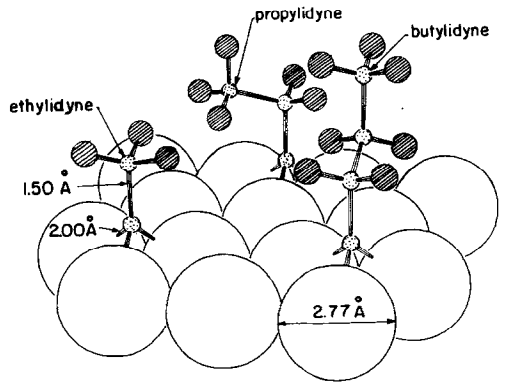

FIG. 19. Atomic structures for ethylidyne, propylidyne, and butylidyne chemisorbed on Pt(111) (*54*).

creasing temperature and decreasing hydrogen pressure as observed experimentally. The apparent activation energy for this process was 11–18 kcal/mol which is typical for polymerization reactions (see, for example, Ref. (*55*)). Since dehydrogenation was always the fastest hydrocarbon conversion reaction, it is tempting to suggest that the nucleation and growth of the carbon deposit results from polymerization of chemisorbed hexenes.

At the lower reaction temperatures (<560 K), the carbon deposit assumed a two-dimensional structure, and the deactivation was simply first order in θ_i. Every molecule incorporated was equally effective in blocking platinum surface sites that were required for skeletal rearrangement reactions and then, $\theta_i = \eta(1 - \theta_c)$. At higher temperatures the deposit gradually converted into a three-dimensional structure (*32*), and this conversion was accompanied by a continuous decrease in the apparent order for the deactivation reaction. It appears that this change in order can be correlated with a charge in morphology of the carbon deposit. The fractional order time dependence indicates that the molecules which were incorporated at high temperatures were not as effective in blocking platinum sites as at the lower temperatures. This is expected if polymerization proceeds at the surface but the deposit continuously rearranges (or decomposes) to restore a certain fraction of the platinum sites that were used for polymerization process.

5. CONCLUSIONS

The structure and temperature dependence of *n*-hexane skeletal rearrangement was investigated near atmospheric pressure over a series of platinum single crystal surfaces with well-defined surface structure and composition. Aromatization of *n*-hexane to benzene displayed unique structure sensitivity in which the rates and selectivities for this important reforming reaction were maximized on platinum surfaces with high concentrations of (111) microfacets. The rates of isomerization, C_5-cyclization, and hydrogenolysis reactions displayed little dependence on platinum surface structure. The distribution of hydrogenolysis products was influenced markedly by terrace structure. Platinum surfaces with (100) terraces favored internal C–C bond scission, whereas surfaces with (111) terraces displayed a higher selectivity for terminal hydrogenolysis.

Selectivities for *n*-hexane skeletal rearrangement varied markedly with temperature and hydrogen pressure. Changes in selectivity with reaction conditions were related to a change in identity of the most abundant surface intermediate that results from a change in the surface concentration of chemisorbed hydrogen. Skeletal rearrangement was dominated by cyclic mechanisms involving both 1,5- and 1,6-ring closure. Polymerization of the adsorbed species competed with skeletal rearrangement and lead to the growth disordered carbonaceous deposits on the platinum surfaces. The primary role of this deposit was that of a nonselective poison.

ACKNOWLEDGMENTS

This work was supported by the Director, Office of Energy Research, Office of Basic Energy Sciences, Materials Sciences Division of the U.S. Department of Energy under Contract DE-AC03-76SF00098.

REFERENCES

1. Paal, Z., "Advances in Catalysis," Vol. 29, p. 273. Academic Press, New York, 1980.
2. Santacessaria, E., Gelosa, D., and Carra, S., *J. Catal.* **39,** 403 (1975).
3. Paal, Z., and Tetenyi, P., *J. Catal.* **29,** 176 (1973).
4. Anderson, J. R., and Shimoyama, Y., "Proceedings, 5th International Congress on Catalysis, Miami, 1972," p. 695.
5. Lankhorst, P. P., DeJongste, H. C., and Ponec, V., *in* "Catalyst Deactivation (B. Delmon and G. C. Froment, Eds.). Elsevier, Amsterdam/New York, 1980.
6. Santacessaria, E., Gelosa, D., Carra, S., and Adami, I., *Ind. Eng. Chem. Prod. Res. Dev.* **17,** 68 (1978).
7. Dautzenberg, F. M., and Platteeuw, J. C., *J. Catal.* **19,** 41 (1970).
8. Dautzenberg, F. M., and Platteeuw, J. C., *J. Catal.* **24,** 264 (1972).

9. DeJongste, H. C., Kuijers, K. J., and Ponec, V., "Proceedings, 6th International Congress on Catalysis, London, 1976," p. 915.
10. Karpinski, Z., and Koscielski, T., *J. Catal.* **63,** 313 (1980).
11. Koscielski, T., Karpinski, Z., and Paal, Z., *J. Catal.* **77,** 539 (1982).
12. Biloen, P., Helle, J. N., Verbeek, H., Dautzenberg, F. M., and Sachtler, W. M. H., *J. Catal.* **63,** 112 (1980).
13. Dautzenberg, F. M., Helle, J. N., Biloen, P., and Sachtler, W. M. H., *J. Catal.* **63,** 119 (1980).
14. van Schaik, J. R. H., Dessing, R. P., and Ponec, V., *J. Catal.* **38,** 273 (1975).
15. Biloen, P., Dautzenberg, F. M., and Sachtler, W. M. H., *J. Catal.* **50,** 77 (1977).
16. Cinneide, A. D., and Gault, F. G., *J. Catal.* **37,** 311 (1975).
17. Ponec, V., and Sachtler, W. M. H., "Proceedings, 5th International Congress on Catalysis, Miami, 1972," p. 645.
18. Plunkett, T. J., and Clarke, J. K. A., *J. Catal.* **35,** 330 (1974).
19. Clarke, J. K. A., Manninger, T., and Baird, T., *J. Catal.* **54,** 230 (1978).
20. Barron, Y., Coronet, D., Maire, G., and Gault, F. G., *J. Catal.* **2,** 152 (1963).
21. Corolleur, C., Tamanova, D., and Gault, F. G., *J. Catal.* **24,** 401 (1972).
22. Amir-Ebrahami, V., Garin, F., Weisang, F., and Gault, F. G., *Nouv. J. Chemie* **3,** 529 (1979).
23. Corolleur, C., Gault, F. G., Juttard, D., Maire, G., and Muller, J. M., *J. Catal.* **7,** 466 (1967).
24. Maire, G., Corolleur, C., Juttard, D., and Gault, F. G., *J. Catal.* **21,** 250 (1971).
25. Dartigues, J. M., Chambellan, A., Corolleur, S., Gault, F. G., Renouprez, A., Moraweck, B., Bosch Giral, P., and Dalmai-Imelik, G., *Nouv. J. Chem.* **3,** 591 (1979).
26. Clarke, J. K. A., and Rooney, J. J., "Advances in Catalysis," Vol. 25, p. 125. Academic Press, New York, 1976.
27. Anderson, J. R., and Avery, N. R., *J. Catal.* **5,** 446 (1966).
28. McKervey, M. A., Rooney, J. J., and Samman, N. G., *J. Catal.* **30,** 330 (1973).
29. Gillespie, W. D., Herz, R. K., Petersen, E. E., and Somorjai, G. A., *J. Catal.* **70,** 147 (1981).
30. Herz, R. K., Gillespie, W. D., Petersen, E. E., and Somorjai, G. A., *J. Catal.* **67,** 371 (1981).
31. Davis, S. M., Zaera, F., and Somorjai, G. A., *J. American Chem. Soc.* **104,** 7453 (1982).
32. Davis, S. M., Zaera, F., and Somorjai, G. A., *J. Catal.* **77,** 439 (1982).
33. Davis, S. M., and Somorjai, G. A., *J. Catal.* **65,** 78 (1980).
34. Davis, S. M., and Somorjai, G. A., *J. Phys. Chem.*, in press.
35. Van Hove, M. A., and Somorjai, G. A., *Surf. Sci.* **92,** 489 (1980).
36. Blakely, D. W., and Somorjai, G. A., *Surf. Sci.* **65,** 419 (1977).
37. Van Hove, M. A., Koestner, R. J., Stair, P. C., Biberian, J. P., Kesmodel, L. L., and Somorjai, G. A., *Surf. Sci.* **103,** 189 (1981); **103,** 218 (1981).
38. Zaera, F., Davis, S. M., and Somorjai, G. A., in press.
39. Davis, S. M., Ph.D. thesis, University of California, Berkeley, 1981.
40. Muller, J., and Gault, F. G., *J. Catal.* **24,** 361 (1972).
41. Garin, F., Aeiyach, S., Legare, L., and Maire, G., *J. Catal.* **77,** 323 (1982).
42. Lu, K. E., and Rye, R. R., *Surf. Sci.* **45,** 677 (1974).
43. Christmann, K., and Ertl, G., *Surf. Sci.* **60,** 211 (1976).
44. McCabe, R. W., and Schmidt, L. D., "Proceedings, 7th International Vacuum Congress and 3rd International Conference Solid Surfaces, Vienna, 1977," p. 1201.
45. Sinfelt, J. H., "Advances in Catalysis," Vol. 23, p. 91. Academic Press, New York, 1973.
46. Davis, S. M., and Somorjai, G. A., "The Chemical Physics of Solid Surfaces and Heterogeneous Catalysis," Vol. 4. Elsevier, Amsterdam, 1982.
47. Leclercq, G., Leclercq, L., and Maurel, R., *J. Catal.* **50,** 87 (1977).
48. Minot, C., Van Hove, M. A., and Somorjai, G. A., *Surf. Sci.* **127,** 441 (1982).
49. Yao, H. C., Yu Yao, Y. F., and Otto, K., *J. Catal.* **56,** 21 (1979).
50. Kesmodel, L. L., Dubois, L. H., and Somorjai, G. A., *Chem. Phys. Lett.* **56,** 267 (1978).
51. Kesmodel, L. L., Dubois, L. H., and Somorjai, G. A., *J. Chem. Phys.* **70,** 2180 (1979).
52. Koestner, R. J., Frost, J. C., Stair, P. C., Van Hove, M. A., and Somorjai, G. A., *Surf. Sci.* **116,** 85 (1982).
53. Kesmodel, L. L., and Gates, J. A., *Surf. Sci.* **111,** L747 (1981).
54. Gavezotti, A., Simonetta, M., Van Hove, M. A., and Somorjai, G. A., *Surf. Sci.* **122,** 292 (1982).
55. Rillmeyer, F. W., Jr., "Textbook of Polymer Science." Wiley, New York, 1971.